Study on incompressible fluid analysis by three-dimensional particle method with finite volume techniques

Shigeyuki Hibi[1,*], *Kazuki* Yabushita[1], and *Takayuki* Tsutsui[1]

[1]The National Defense Academy, Department of Mechanical Systems Engineering, 1-10-20 Hashirimizu, Yokosuka, Kanagawa 239-8686, Japan

Abstract. Simulating violent free-surface flows by particle methods is effective. In recent years, the SPH (Smoothed Particle Hydrodynamics) method and the MPS(Moving Particle Simulation method) method are considered representative especially in the fields of ship engineering and civil engineering but these methods need various artificial parameters in calculation and may have unnatural large numerical oscillation in the calculated pressure values. In order to avoid these problems, the authors have proposed another particle method based on the finite volume techniques. The usefulness of the proposed method in two-dimensional problems has been verified by comparing the pressure fluctuation when a water tank of the two-dimensional model is forcibly oscillated with the corresponding experiment [1]. Therefore, in this research, the authors extended the algorithm so that the calculation formula can be applied to three-dimensional problems. The effectiveness of the calculation is demonstrated by applying to the dam break problem.

1 Introduction

Incompressible fluid analysis using particle methods is effective for flows with large fluid deformations, such as when a liquid such as ballast water or LNG/LPG ships strikes a wall of tank in a ship, or when a wave breaks up after a wave rides on a ship. In recent years, the SPH[2] method (Smoothed Particle Hydrodynamics) and the MPS[3] method (Moving Particle Simulation method) have attracted attention in the fields of ship engineering and civil engineering, but these methods need various artificial parameters in calculation and may have unnatural large numerical oscillation in the calculated pressure values. In order to avoid these problems, the authors have proposed another particle method [4] based on the finite volume techniques. In this particle method, the equation of continuity and the N-S equation are transformed into forms that are easy to adapt to the particle method. Based on the finite volume techniques the boundary condition is uniformly treated so that particles can freely move not only on the free surface but also in the air, whereas SPH [5] and MPS [6] methods need some special treatments. Through the research up to last year, the usefulness of the proposed method in two-dimensional problems has been verified by comparing the pressure fluctuation when a water tank of the two-dimensional model is forcibly oscillated with the corresponding experiment. Therefore, in this research, the authors extended the algorithm so that the calculation formula can be applied to three-dimensional problems. The effectiveness of the proposed method is validated by comparison with the dam break experiment executed by the authors refering to the experiment by Zhou [7]. The dam break problem is usually used for a benchmark problem. By comparing the time history of pressure values occured on the wall with the experimental results, the effectiveness of the proposed particle method was assured.

2 Numerical simulation by three-dimensional particle method with finite volume techniques

In particle methods, fluid is modeled as a collection of particles and discretized by considering the interaction between particles without a calculation lattice. Therefore, particle methods are suitable for intense fluid analysis with strong nonlinearity.

2.1 Discretization with finite volume techniques

The fundamental equations described by a fluid particle coordinates $\hat{r}$ are represented by the Navier–Stokes equations and the continuity equation.

$$\left.\frac{\partial \boldsymbol{v}}{\partial t}\right|_{\hat{r}} = -\frac{1}{\rho}\hat{\nabla}p + \boldsymbol{K} + \nu\hat{\nabla}\cdot\hat{\nabla}\boldsymbol{v} \tag{1}$$

$$\hat{\nabla}\cdot\hat{\nabla}p = \rho\lim_{\Delta\to 0}\frac{\hat{\nabla}(t,\hat{r})\cdot\boldsymbol{v}(t-\Delta t,\hat{r}-\Delta\hat{r})}{\Delta t} \tag{2}$$

Here $\boldsymbol{v}$ is the speed of particles, p is the pressure of particles, ρ is the density of fluid, $\boldsymbol{K}$ is outer forces and ν is the kinematic coefficient of viscosity of fluid. From

* Corresponding author: hibiteru@nda.ac.jp

Gauss's theorem equations (1) and (2) are transformed into flow equations of integral shape.

$$\left.\frac{\partial \boldsymbol{v}}{\partial t}\right|_{\hat{r}} = -\lim_{V\to 0}\frac{1}{\rho V}\int_S p\boldsymbol{n}dS + \boldsymbol{K} + \lim_{V\to 0}\frac{\nu}{V}\int_S \frac{\partial \boldsymbol{v}}{\partial n}dS \quad (3)$$

$$\lim_{V\to 0}\frac{1}{V}\int_S \frac{\partial p}{\partial n}dS = \lim_{\substack{\Delta t\to 0\\ V\to 0}}\frac{\rho}{V\Delta t}\int_S \boldsymbol{v}(t-\Delta t)\cdot\boldsymbol{n}dS \quad (4)$$

Here $\boldsymbol{n}$ is the normal vector of a particle and $\boldsymbol{V}$ is the volume of a particle.

Eventually, the discritized equations are derived from equations (3) and (4) in the proposed method.

$$\boldsymbol{v_i} - \frac{\Delta t\nu}{\frac{4}{3}\pi R^3}\sum_{j=1,j\neq i}^{N}\frac{\boldsymbol{v_j}-\boldsymbol{v_i}}{r_{ij}}\Delta S_{ij} \quad (5)$$
$$= {\boldsymbol{v_i}}^{n-1} - \frac{\Delta t}{\frac{4}{3}\pi R^3}\sum_{j=1,j\neq i}^{N}\left(p_i + (p_j-p_i)\frac{R}{r_{ij}}\right)\boldsymbol{n_{ij}}\Delta S_{ij} + \boldsymbol{X}\Delta t$$

$$\sum_{j=1,j\neq i}^{N}\frac{\boldsymbol{p_j}-\boldsymbol{p_i}}{r_{ij}}\Delta S_{ij} - \frac{p_i}{R}(4\pi R^2 - S_i) \quad (6)$$
$$= \frac{\rho}{\Delta t}\sum_{j=1,j\neq i}^{N}\left({\boldsymbol{v_i}}^{n-1} + ({\boldsymbol{v_j}}^{n-1} - {\boldsymbol{v_i}}^{n-1})\frac{R}{r_{ij}}\right)\boldsymbol{n_{ij}}\Delta S_{ij} - \frac{\rho}{\Delta t}{\boldsymbol{v_i}}^{n-1}\cdot\boldsymbol{S_i}$$

Here

$$\begin{aligned}
\boldsymbol{r_i} &= (x_i, y_i, z_i)\\
\boldsymbol{r_{ij}} &= \boldsymbol{r_j} - \boldsymbol{r_i}\\
r_{ij} &= \sqrt{(x_j-x_i)^2 + (y_j-y_i)^2 + (z_j-z_i)^2}\\
\boldsymbol{n_{ij}} &= \frac{\boldsymbol{r_{ij}}}{r_{ij}}\\
R &= \frac{D}{\sqrt[3]{\frac{3}{4}\pi}}
\end{aligned}$$

$$\boldsymbol{S_i} = \sum_{j=1,j\neq i}^{N}\boldsymbol{n_{ij}}\Delta S_{ij}, S_i = \sum_{j=1,j\neq i}^{N}\Delta S_{ij}$$
$$\boldsymbol{K} = (0,0,-g)$$

$$\Delta S_{ij} = 4\alpha\frac{r_e - r_{ij}}{r_e - D}R^2 d\theta_{ij}d\phi_{ij}$$
$$\alpha = \frac{4\pi R}{\sum_{j=1,j\neq i}^{N}4\frac{r_e-r_{ij}}{r_e-D}R^2 d\theta_{ij}d\phi_{ij}} = \frac{\pi}{\sum_{j=1,j\neq i}^{N}\frac{r_e-r_{ij}}{r_e-D}Rd\theta_{ij}d\phi_{ij}}$$

Subscript i means the particle number of interest and subscript j means the neighboring particle number of the particle i. Superscript n indicates the time step number. $\boldsymbol{r}_i$ means position vector of the i-th particle. The particles are assumed to be spherical (just round in the two dimensional model) and the influence of the neighboring particle j to the particle i is carried out through the micro surface area ΔS_{ij} expressed by equation (7) according to the concept of the Finite Volume Method.

R stands for the radius of a particle and satisfies the following equation.

$$\frac{4}{3}\pi R^3 = D^3 \quad (8)$$

D is the average inter-particle distance and is determined by the spatial resolution of the calculation model. This parameter corresponds to the smoothing length h in the SPH[2] method and the effective radius in the MPS method.

Considering the efficiency and stability of calculation, it is considered that neighboring particles far from the 'effective radius' r_e named in the MPS method, do not have a effect. In this study the following vallue is adopted for the parameter r_e as same as the MPS method.

$$r_e = 3.1\,D \quad (9)$$

g is the gravity acceleration and in this study the outer force is only the gravity. The pressure value of particles at each time step is obtained by implicitely solving the equation (6) using the PCGS method (Preconditioned Conjugate Gradient Squared method). The velocity value of particles is also obtained from the equation (5) implicitly using the PCGS method in case of considering viscosity of fluid and explicitly in case that viscosity is not taken into consideration.

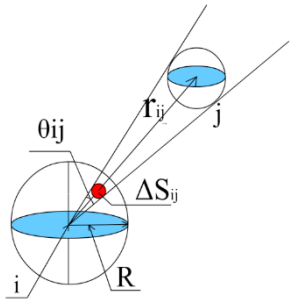

Fig. 1. Micro surface area ΔS_{ij} between particle i and particle j.

3 Dam break experiment

3.1. Specification of the apparatus

The apparatus for the dam break experiment was made by the authors refering to Zhou [4]'s model (See Figs. 2 and 3). The size of Zhou's apparatus is relatively bigger than other researcher's one in order to ignore the effect of the surface tension sufficiently because their study field is in the naval architecture. The authors determined almost half size of Zhou's one considering both the production cost and production time.

The size of tank is $590\times 1620\times 300$ (mm) (Height $\times$ Width $\times$ Depth). At the beginning of a experiment, water is sotred in the left side of the tank devided by the flap and right side of the tank is empty. Water depth is 300 mm.

A pressure sensor is attached on the right side wall of the tank mounted on the apparatus. The position of the sensor is 40 mm or 80 mm from the bottom. The pressure receiver has round area with diameter of 8 mm. When the

weight connected to the flap by a tough rope is fallen and the flap is lifted, the water column starts to collapse and it will cause a impact force on the right side wall of the tank. We measured time histories of this pressure on the wall repeatedly.

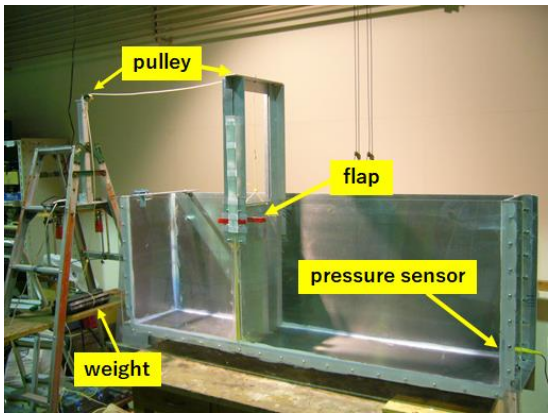

Fig. 2. Dam breaking apparatus overview.

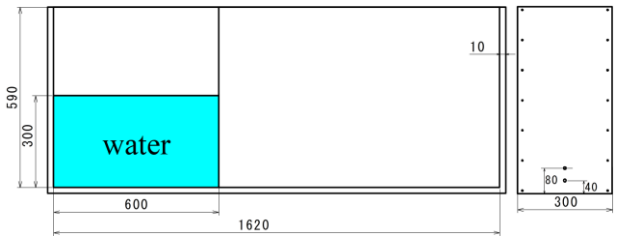

(mm)

Fig. 3. Dimensions of the dam breaking apparatus.

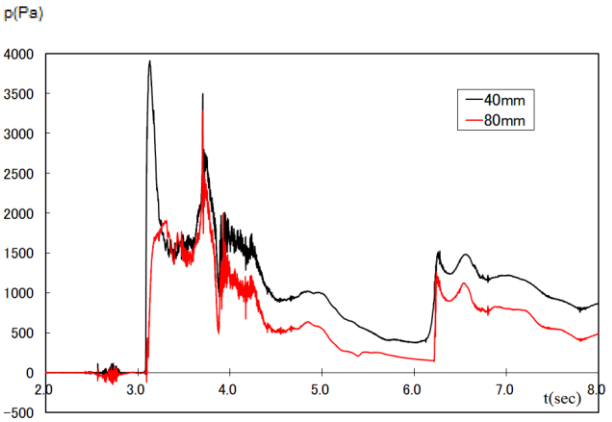

Fig. 4. Time history of pressure on the right side of the tank.

Fig. 4 shows a typical experimental result about time history of pressure on the right side of the tank. The red and black curves represent values of the pressure sensors mounted 40mm and 80mm from the bottom each other. From the figure, it can be seen that there is not much difference in the timing of the first and second impacts and the dam break is a steep and violent phenomenon.

Fig. 5 shows a comparison with time history of pressure between the Zhou's experimental result and ours at the corresponding position, 160mm and 80mm each other. Eventhough the diameter of pressure sensors are so differnt between Zhou and us, 90mm and 8mm each other, the time history of pressure is so similar except the peak values in impact.

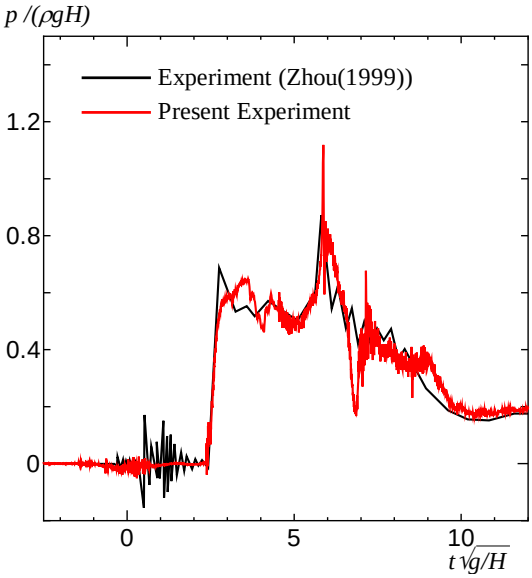

Fig. 5. Comparison with time history of pressure.

3.2 Estimation of the confidence intervals based on the *t*-distribution and uncertainty analysis

Independent random variables subject to the normal distribution $X_1, X_{2,\ldots} X_N$ are assumed that mean values are μ and variances are σ^2 (usually unkonwn). In case of a sample of size N the confidence interval at a confidence level z % is given by eq. (10).

$$\bar{x} - t_{N-1}(z\%)\frac{u}{\sqrt{N}} \le \mu \le \bar{x} + t_{N-1}(z\%)\frac{u}{\sqrt{N}} \quad (10)$$

Fig. 6 shows the moved distance of the flap in 0.2 second. Error bars mean to the cconfidence interval of 95%. Fig. 7 and 8 show time average of pressure values for 2 seconds by eq. (11) at both 40mm and 80mm positions from the bottom on the right side of the tank.

$$\int_0^2 p dt / 2 \quad (11)$$

From these figures the 8th experiment seemes to be different from other experiments, possibly differences in how the weight falls. However, error bars of ttime average of pressure values at both positions tend to decrease. This implies that there is no significant difference in the evaluation of the impact force on the wall, considering the integrated value of time average.

Uncertainty analysis was also carried out according to the GUM (Guide to the Expression of Uncertainty in Measurement) guidance. The expanded uncertainty calculated from Table 1(at the last of the paper) is 31.9 (Pa).

The number of iterations used here is 11 times. From this result, it can be seen that the pressure variation is not so large as compared with the pressure fluctuation on the wall surface.

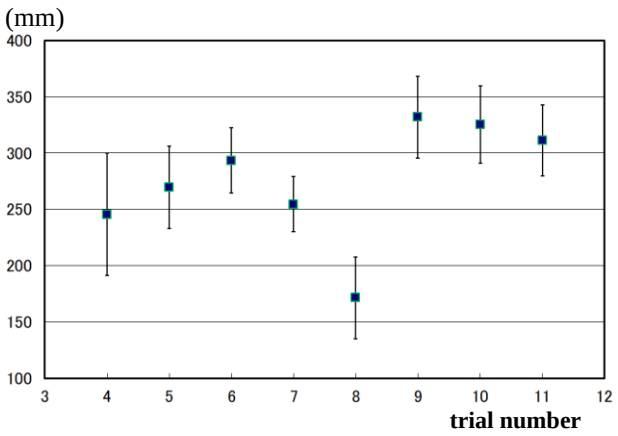

Fig. 6. Moved distance of the flap in 0.2 seconds.

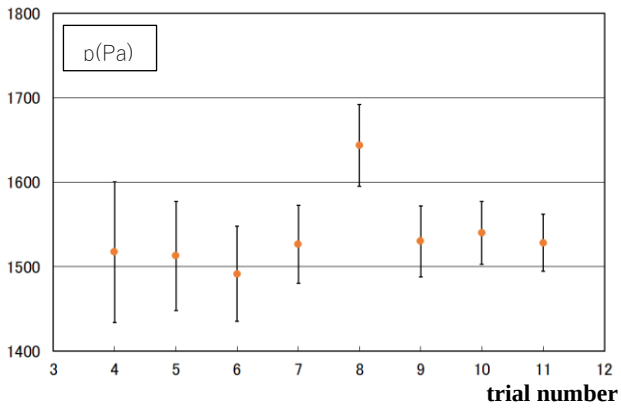

Fig. 7. Time average of pressure values (40mm).

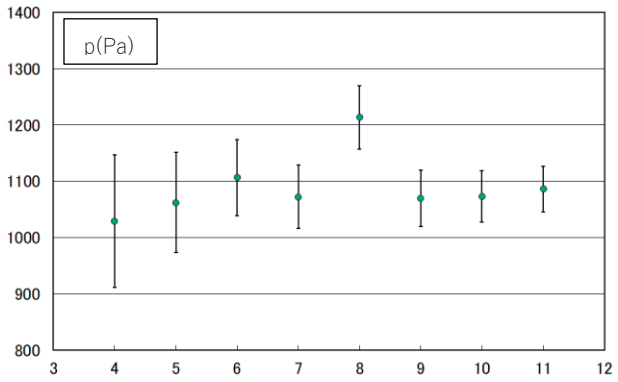

Fig. 8. Time average of pressure values (80mm).

4 Numerical simulation and discussion

4.1 Comparison of calculation accuracy of the particle method with static pressure

At first we confirm accuracy of the proposed particle method by static pressure. In Fig. 9 a tank model for still water is shown. Water depth is 0.3 m as same as the dam break experiment. The total particle number is 7,901.The average inter-particle distance D is 38.10 mm.

Numerical simulation was carried out with the time step of 0.0001 sec. in all cases. The CPU of PC used for the simulation is i7 (2.9 GHz) and the memory of the PC is 3 Gbytes. Fig. 10 shows the time history of static pressure at the bottom of the tank. The pressure value is derived from just one particle at the bottom of the tank. We can see some fluctuations for the first few seconds in simulation time and after that the pressure values become fairly stable. These fluctuations of pressure at the beginning occur when relative position of particles turns stabler and closer from the initial particle arrangement in a tetragonal lattice.

In order to avoid the fluctuation of pressure value, the particle layout of this still water after enough simulation time is used for the initial particle layout of the dam break simulation later.

Fig. 11 shows hydrostatic pressure distribution to whole water particles in depth direction. The red line and blue line respectively represent the hydrostatic linear curve and the analytic pressure value of the bottom of tank. From this figure, we can see that there are some particles with different pressures, but as a result, the hydrostatic pressure at the bottom can be estimated well by the least squares method.

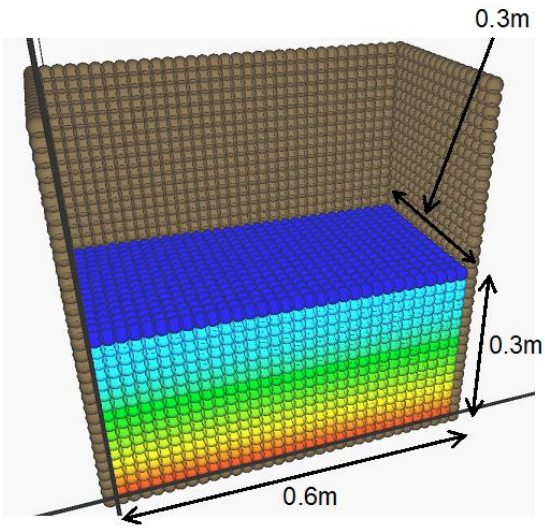

Fig. 9. Initial particle arrangement for still water simulation.

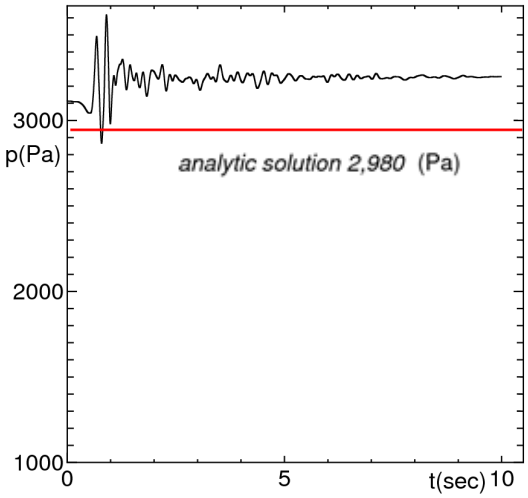

Fig. 10. Time history of static pressure at the bottom of tank.

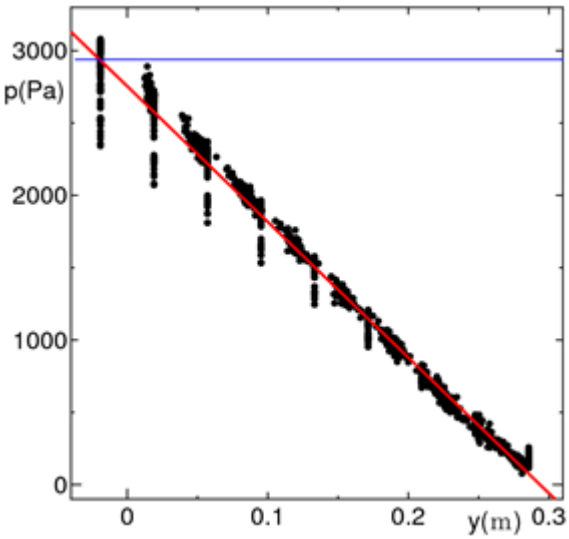

Fig. 11. Hydrostatic pressure distribution in depth direction.

4.2 Numerical Simulation of dam break experiment

We prepared two models, named X2(13,855 particles) and X4(51,209 particles). The average inter-particle distance *D* of the X4 model is half length for the one of the X2 model. The initial particle arrangement for X2 model is shown in Fig. 12. The drawing is made by the OpenGL. The front wall is present but not drawn to observe easily particle movements.

Numerical simulation was carrid out under the same conditions as the still water experiment in the section 4.2. The appearance of the simulation for X4 model is shown from Fig. 13(a) to Fig. 13(e). The gradation of the particle colors represents the magnitude of the pressure value from blue to red.

The pressure values obtained by particle methods generally fluctuate in time and space domains and then in order to obtain a stable pressure values without fluctuation some numerical tecniques are often used. In this study we introduced a numerical filter for pressure value every time step. The filter simply takes an average value of 500 steps before and after the pressure value every moment.

From these figures it can be seen that the water column collapses smoothly and hit the right side wall of the tank and intense impulsive force can occure on the wall.

Fig. 14 shows comparison of the experiment and simulation results for time history of pressure value at the position where the pressure sensor is attached.

From this result, it can be seen that the numerical results for each models have good agreement with the experiment except the peak value. The reason for this is due to the relation between the area of the pressure sensor and the spacial resolution in the simulation. While the diameter of the pressure sensor is 8mm, the average inter-particle distance D is 38.10 mm in the X2 model and 19.05 mm in the X4 model. Further study should be needed for this problem.

However, even though the number of particles is less, it is observed that the accuracy of the analysis is similar. This shows the superiority of the proposed particle method in three-dimensional simulation.

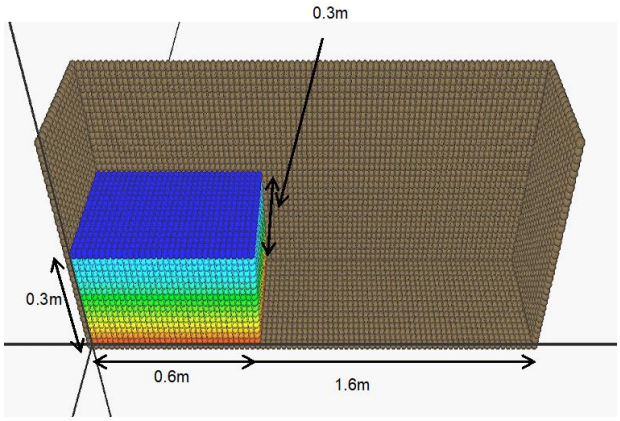

Fig. 12. Initial particle arrangement for dam break simulation (X2 model).

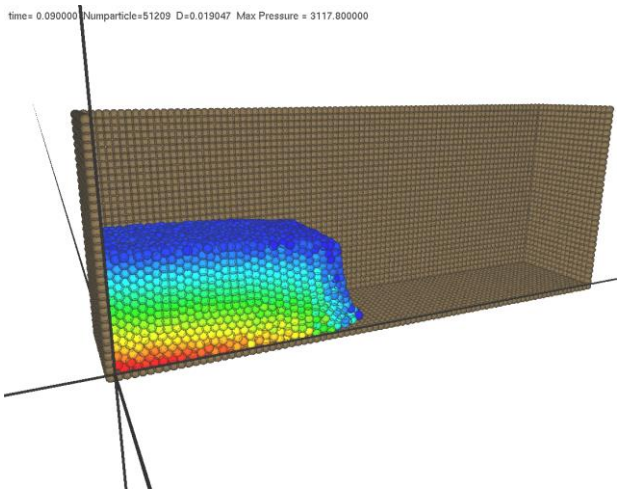

Fig. 13(a). Bird's eye view of dam break simulation (t = 0.09 sec.).

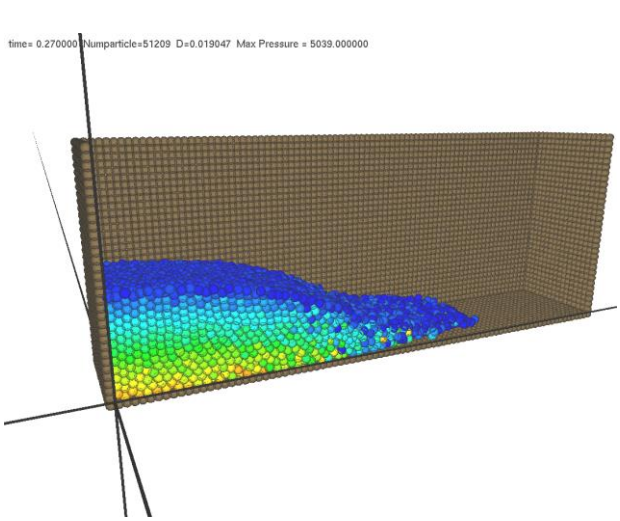

Fig. 13(b). Bird's eye view of dam break simulation (t = 0.27 sec.).

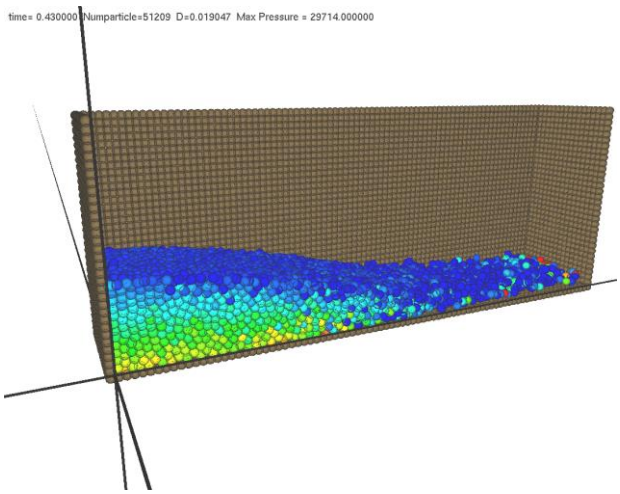

Fig. 13(c). Bird's eye view of dam break simulation (t = 0.43 sec.).

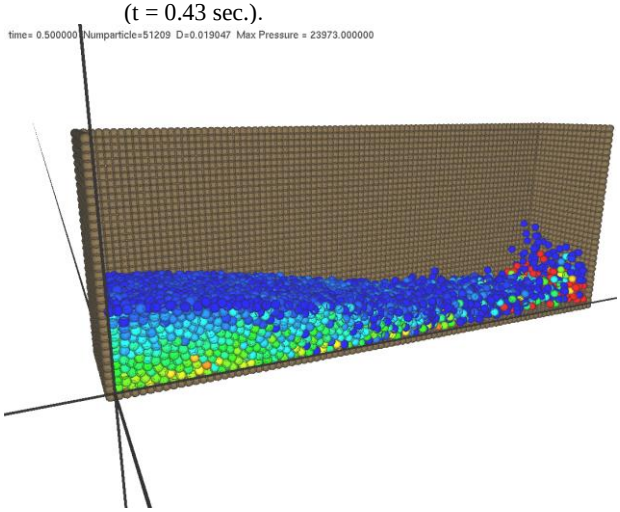

Fig. 13(d). Bird's eye view of dam break simulation (t = 0.50 sec.).

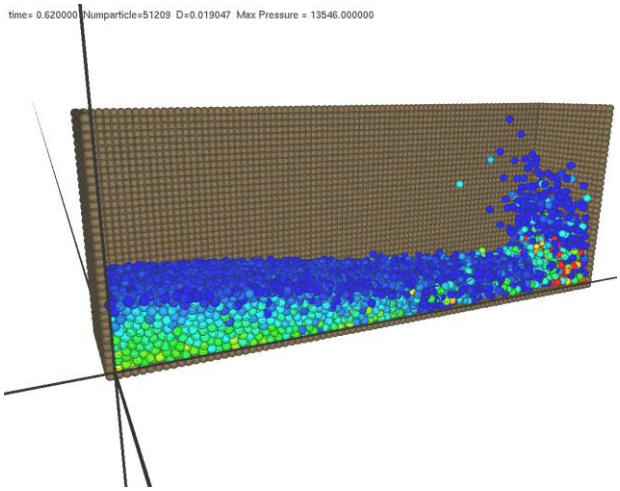

Fig. 13(e). Bird's eye view of dam break simulation (t = 0.62 sec.).

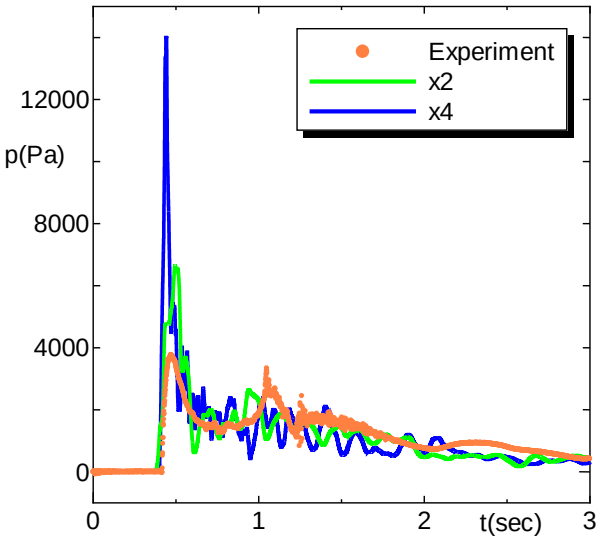

Fig. 14. Time history of pressure at the 40mm position from the bottom on the right side wall.

5 Conclusion

In this study the authors carried out the dam break experiment at first and then validate the proposed numerical method comparing the experimental results. Some consideration were found about it as below.

- Effectiveness of the proposed three-dimensional particle method is assured through the numerical simulation of intense non-linear phenomena.
- Even less number of particles can simulate the impulsive pressure value in the dam break problem by the proposed method.

References

1. Shigeyuki Hibi, EPJ Web Conf. **180**, 02034 (2018)
2. J.J.Monaghan, Journal of Computational Physics **110**, 2, 399(1994)
3. Koshizuka S, Oka Y. Moving-particle semi-implicit method for fragmentation of incompressible fluid. Nucl. Sci. Eng. ,**123**:421–34. (1996)
4. Shigeyuki Hibi and Kazuki Yabushita, ACC J., Vol. **25** Issue 1(2019)
5. Xingye Ni, Jinyu Sheng, Weibing Feng, Journal of Atmospheric and Oceanic Technology, Vol. **33**, 11, 2435 -2460 (2016)
6. Gen Li, Jinchen Gao, Panpan Wen et al., Computer Methods in Applied Mechanics and Engineering, Vol. 367 ,(2020) 113116
7. Z.Q. Zhou, J.O. De Kat and B. Buchner, *Proc. 7th Int. Conf. Num. Ship Hydrod.*, **5.1 1**(1999)

Table 1. Budget table for estimation of uncertainty concerning the pressure value at 40mm position from the bottom.

marks	factors of uncertainty	cause of uncertainty	type of uncertainty	probabilistic distribution	mean value	sensitivity factor $\frac{\partial f}{\partial x_i}$	standard uncertainty		
ρ	density of water	water temperature	A	normal	9.99E-01	871	6.62E-05		
a	Coefficient for conversion	repeated experiment	A	normal	87.96	9.9	0.342		
$V(0)$	Voltage value against atmospheric pressure	repeated experiment	A	normal	1.63	-861	1.53E-02		
$V(100)$	voltage value at the 100mm water depth	repeated experiment	A	normal	2.64	861	2.16E-02		
V_p	calibration of the pressure sensor	calibration error of the pressure sensor	B	uniform		1.0	1.62		
V_{amp}	calibration of the amplifier	calibration error of the amplifier	B	uniform		1.0	4.98		
u_c	combined standard uncertainty							16.0	(Pa)
u	expanded uncertainty							31.9	(Pa)